Soft Matter

PAPER

View Article Online
View Journal | View Issue

Cite this: *Soft Matter*, 2017, **13**, 1702

Influence of fluid viscosity and wetting on multiscale viscoelastic lubrication in soft tribological contacts†

Nichola Selway, Vincent Chan and Jason R. Stokes*

Friction (and lubrication) between soft contacts is prevalent in many natural and engineered systems and plays a crucial role in determining their functionality. The contribution of viscoelastic hysteresis losses to friction in these systems has been well-established and defined for dry contacts; however, the influence of fluid viscosity and wetting on these components of friction has largely been overlooked. We provide systematic experimental evidence of the influence of lubricant viscosity and wetting on lubrication across multiple regimes within a viscoelastic contact. These effects are investigated for comparatively smooth and rough elastomeric contacts (PTFE–PDMS and PDMS–PDMS) lubricated by a series of Newtonian fluids with systematically controlled viscosity and static wetting properties, using a ball-on-disc tribometer. The distinct tribological behaviour, characterised generally by a decrease in the friction coefficient with increasing fluid viscosity and wettability, is explained in terms of lubricant dewetting and squeeze-out dynamics and their impact on multi-scale viscoelastic dissipation mechanisms at the bulk-, asperity-, sub-asperity- and molecular-scale. It is proposed that lubrication within the (non-molecularly) smooth contact is governed by localised fluid entrapment and molecular-scale (interfacial) viscoelastic effects, while additional rubber hysteresis stimulated by fluid–asperity interactions, combined with rapid fluid drainage at low speeds within the rough contact, alter the general shape of the Stribeck curve. This fluid viscosity effect is in some agreement with theoretical predictions. Conventional methods for analysing and interpreting tribological data, which typically involve scaling sliding velocity with lubricant viscosity, need to be revised for viscoelastic contacts with consideration of these indirect viscosity effects.

Received 26th October 2016,
Accepted 29th January 2017

DOI: 10.1039/c6sm02417c

rsc.li/soft-matter-journal

1. Introduction

The study of soft-contact friction and lubrication is of great relevance to our fundamental understanding of biotribology and biological interface mechanics, but also has wide-reaching practical application in the design of bio-mimetics,[1] bio-inspired adhesives, biomedical devices *e.g.* prostheses,[2] rubber sealants,[3] and shaving devices. Tribological interactions at the tongue-palate and skin interfaces are also considered to play a key role in determining the functionality, including tactile perception, of food/beverages and personal care products (*e.g.* cosmetics, skin creams).[4–7]

The tribological response of a lubricated system is determined by both hydrodynamics and surface contact forces. These two friction mechanisms are often considered in isolation (as discrete components) despite the complex interplay that exists between them. For example, under hydrodynamic (full-film) lubrication conditions, where the fluid pressure and lift force generated are sufficient to separate the opposing surfaces, the viscous drag of the lubricant is often considered to be the primary contributor to the friction force. However, fluid pressure acting on soft substrates can induce viscoelastic hysteresis losses that also contribute significantly to friction.[8,9] Similarly, and perhaps more critically, the full extent of the role of lubricant viscosity in what is conventionally considered the 'boundary' and 'mixed' regimes has largely been overlooked in the case of compliant, viscoelastic contacts. We seek to address this oversight and emphasise its importance in the interpretation of tribological data.

It is widely accepted that the transition through different lubrication regimes occurs as a function of the 'reduced velocity', $U\eta$ (entrainment speed or sliding velocity multiplied by lubricant viscosity), which is also considered as the shear stress intensity acting across the contact zone, with units Pa m

School of Chemical Engineering, The University of Queensland, Brisbane 4072, Queensland, Australia. E-mail: jason.stokes@uq.edu.au, nichola.selway@uqconnect.edu.au; Fax: +61 (0) 7 3365 4199; Tel: +61 (0) 7 3365 4361

† Electronic supplementary information (ESI) available. See DOI: 10.1039/c6sm02417c

or N m^{-1}. This characteristic parameter is a simplified version of the dimensionless Sommerfeld number $\left(\frac{\eta UR}{W}\right)$ or elasto-hydrodynamic number $\left(\frac{\eta UE^{1/3}R^{5/3}}{W^{4/3}}\right)$, for a particular tribo-system with defined (constant) sphere radius R, applied load W, and elastic modulus E. Thus it has become standard practice to interpret and present tribological data in the form of a Stribeck curve, with the friction coefficient as a function of $U\eta$. The term 'Stribeck curve' was originally developed for hard contacts to describe the frictional variation in the entire range of lubrication, including the hydrodynamic, mixed and boundary lubrication regimes. As this paper highlights, caution should be exercised when applying these conventional terms in soft-contact tribology, where lubrication regimes are less well-defined. However, for simplicity, the term 'Stribeck curve' is used here to refer to the overall friction profile for each lubricant.

The apparent collapse of tribological data for different viscosity fluids onto a single master curve by scaling with lubricant viscosity has been reported in many previous studies involving viscoelastic contacts. This master curve is often then used as a reference or baseline when comparing and interpreting the tribological behaviour of other more complex lubricants, such as multiphase fluids, or those containing adsorbent species.[10] For such comparison, there is the assumption that any deviation from the master Stribeck curve can be attributed to non-hydrodynamic effects, such as adsorption and boundary layer formation[11] and/or preferential entrainment or exclusion of particles in multiphase systems.[12–15] This has the potential to be a very powerful interpretive tool as it provides information about the fluid behaviour and composition localised in the contact zone. The same principle has also been used to estimate the average local shear rate and effective viscosity of non-Newtonian lubricants in the contact zone.[11,16] However, the underlying assumption that viscous effects are essentially 'normalised' through scaling with lubricant viscosity is not necessarily valid, leading to potential misinterpretation of tribological data. Therefore, it is necessary to develop new scaling laws for tribological analysis that incorporate the true effect of viscosity on friction and lubrication. We present experimental evidence and analysis on the influence of fluid viscosity and surface roughness on friction and lubrication in a viscoelastic contact. This work focusses on the mixed rolling and sliding tribological contact between a rigid sphere and a viscoelastic half space (*i.e.* ball-on-disc), lubricated by Newtonian fluids with varying viscosities.

There are two key reasons why the effect of viscosity has been overlooked in previous tribological studies involving viscoelastic contacts. Firstly, the friction coefficient is typically plotted on a log scale in order to observe the three lubrication regimes across a range of entrainment speeds. However, this renders it more difficult to visually distinguish between different viscosity lubricants (even when statistically significant differences may exist); hence an apparent collapse of data onto a single master curve is observed and reported. Secondly, the majority of experimental studies on lubrication within a viscoelastic contact use two opposing polydimethylsiloxane (PDMS) surfaces, owing to the material's well-defined surface chemistry, elastomeric properties and biocompatibility. However, a PDMS–PDMS contact has a very high Coulombic (interfacial) friction. This component of the friction coefficient is dominant and the effect of lubricant viscosity on the overall Stribeck curve is less pronounced, though still evident for rough contacts, as noted by Bongaerts *et al.*[10]

In this study, we utilise both the standard PDMS–PDMS tribo-contact, as well as a tribo-system that exhibits a comparatively low Coulombic friction – polytetrafluoroethylene (PTFE) ball on PDMS disc – in order to clearly demonstrate the influence of lubricant viscosity on rubber hysteresis effects, as well as its impact on squeeze-out and dewetting dynamics; that is, beyond its direct contribution to friction in the form of fluid viscous losses. Firstly, we investigate the lubricating properties of binary glycerol–water mixtures, which vary in their viscosity (dynamic properties), but exhibit relatively little variation in their surface tension and static contact angle (equilibrium parameters). We then study two series of ternary glycerol–ethanol–water systems which each span a wide range of static contact angles, while maintaining similar fluid viscosities. Through this systematic variation of fluid viscosity and contact angle, we provide a better mechanistic understanding of the role of lubricant viscosity and dynamic dewetting on viscoelastic lubrication in soft contacts. An empirical model is fitted to the tribological data to obtain model parameters that describe the unique shape of each Stribeck curve. The model parameters are analysed as a function of lubricant viscosity, contact angle and surface roughness, and the findings are discussed in terms of the four constituents of friction defined by Scaraggi and Persson's[17] theory described below. This paper aims to validate aspects of their theoretical model, as well as highlight and address the potential for mis-interpretation of experimental data due to a lack of integration with theoretical and numerical prediction.

2. Background

During rubbing (dry) contact, friction forces are considered to arise from the breaking of adhesive bonds formed at the contact interface,[18,19] as well as subsurface deformation resulting from lateral motion and normal load.[20,21] The latter constitutes an internal (cohesive) friction component relating to the viscoelastic dissipation of stressed molecules in the bulk material, commonly referred to as 'viscoelastic hysteresis losses' or 'deformation losses'.[22,23] For highly compliant tribo-surfaces (*e.g.* elastomers), this internal cohesion is comparable to the interfacial adhesion and both dissipation processes have a significant contribution to the overall friction.[24] Homogenised contact mechanics theories have recently enabled the effective calculation of hysteretic rubber friction for real (multi-scale) rough contacting surfaces. However, studies of friction involving viscoelastic solids have primarily focused on the contact mechanics of dry interacting surfaces, hence the influence of lubricant properties on hysteresis losses has only very recently been considered. Based on theoretical modelling of lubrication within viscoelastic contacts, Scaraggi and Persson[17]

extended the pioneering work of Hooke and Huang[8] and Elsharkawy[9] to show that viscoelastic hysteresis generates an asymmetric fluid pressure field which can affect the Stribeck curve over a wide range of sliding speeds and lubrication regimes.

For lubricated soft contacts, four discrete components of friction need to be considered, as defined in Scaraggi and Persson's[17] model:

(i) solid-contact sliding friction, μ_{Sc}
(ii) solid-contact rolling friction, μ_{Rc}
(iii) wet-contact sliding friction, μ_{Sf}
(iv) wet-contact rolling friction, μ_{Rf}.

The solid-contact sliding and rolling friction components represent the interfacial (adhesive) shear stress and rubber deformation losses, respectively, as mentioned earlier for dry contacts. Wet-contact sliding friction arises from shear stresses generated within the fluid contact regions and includes the contribution from both Poiseuille and Couette flow, while wet-contact rolling friction arises from a combination of fluid viscous losses and fluid-induced rubber deformation losses.

It is necessary to clarify a potential source of confusion here regarding the definition of rolling friction, which is considered to exist even for a pure sliding contact (200% slide-to-roll ratio, SRR). The term 'rolling friction' in this context simply represents the non-elastic effects that occur over the entire contact. For viscoelastic lubrication, this comprises rubber hysteresis losses as well as plastic deformation (fluid viscous losses). This is rationalised by considering that friction measured for a pure sliding contact that exhibits extremely low interfacial shear stress is (almost) equivalent to pure rolling friction.[25]

Scaraggi and Persson[17] modelled each of these friction components as a function of reduced velocity, shown in Fig. 1A and B for a low and high viscosity lubricant respectively. The summation of these four friction component curves yields the Stribeck curve (represented by the red line). The Stribeck curve is divided into distinct regions (denoted by the numbers 1 to 5), which are defined by both the rubber-to-glassy transition of the viscoelastic solid, and the prevalence of wet- *versus* solid-contact friction.

The rubbery region (1) occurs at low reduced velocities where the contact stress stored in the elastomer is capable of relaxing before an asperity can slip to the next contact site. The characteristic peak in solid-contact rolling friction defines the onset of the transition region (2) and is governed by the viscoelastic properties of the solid material. From dry elastomeric studies, this corresponds to the maximum in the loss modulus for smooth contacts and the maximum in the loss tangent for rough contacts.[23] Above the critical velocity, the material is unable to fully relax before the asperities are driven to the next contact site; hence the solid-contact rolling friction decreases as a result of fewer dissipative relaxation events.[24] The glassy region (3–5) occurs when the strain rate (governed by the sliding velocity) is too high for any molecular relaxation of the solid, meaning that there is no longer a contribution from the solid-contact rolling friction.

The classification of boundary (BL), mixed (ML) and hydrodynamic (HL) lubrication is dictated by the dominance of solid-contact friction (BL), the dominance of wet-contact friction (ML), or pure wet-contact friction (HL). As expected, the model

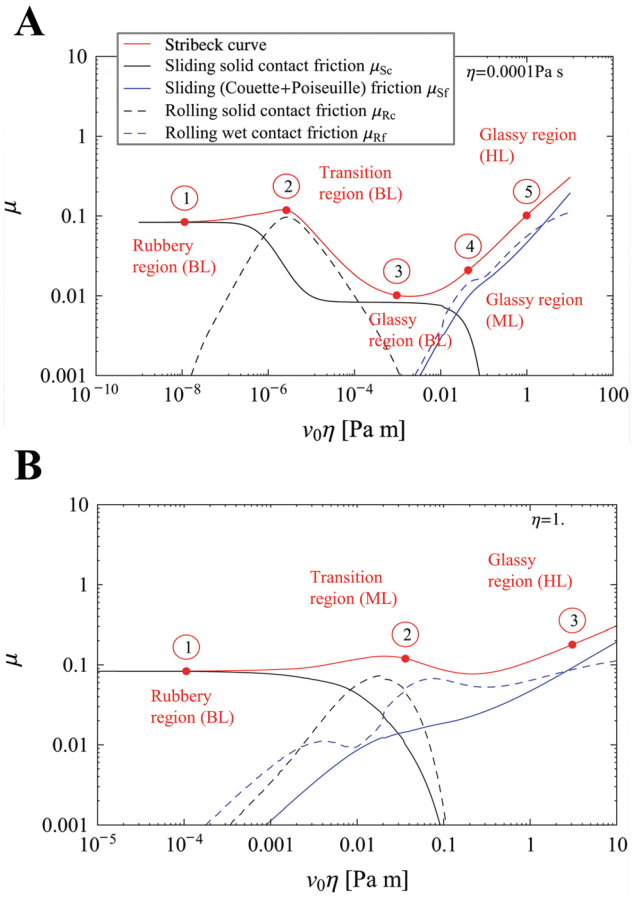

Fig. 1 Scaraggi and Persson's theoretical model for viscoelastic lubrication for a (A) low and (B) high viscosity lubricant, showing the four key components of friction and their summation which yields the Stribeck curve (red). Several distinct regions of the Stribeck curve (numbered 1 to 5) can be identified by superimposing these component curves. Reprinted from Scaraggi and Persson[17] with permission from Elsevier, with minor adaptations.

predicts that solid-contact friction dominates the Stribeck curve at low values of reduced velocity, whereas wet-contact friction has the greatest contribution at high reduced velocities where the conditions facilitate lubricant entrainment.

More interestingly, the model predicts that lubricant viscosity affects the relative contribution of solid-contact *versus* wet-contact friction across the range of reduced velocities, which can alter the shape of the Stribeck curve. This is evidenced by comparing Fig. 1A and B, which demonstrates that the convention of scaling with lubricant viscosity is insufficient to achieve a master curve for lubrication in a viscoelastic contact. According to the model, an increase in lubricant viscosity stimulates additional rubber hysteresis due to fluid pressure acting on the asperities, leading to an increase in the wet-rolling friction (with respect to the wet-sliding friction). In rough contacts, these fluid–asperity interactions can occur at low reduced velocities, such that the wet-contact rolling curve coincides with the solid-contact rolling curve. The overlapping of these friction component curves (as observed in Fig. 1B), alters the shape of the Stribeck curve, including a shift in peak friction to higher values of reduced velocity.

3. Materials and methods

3.1. Tribo-surfaces

Four different tribo-pairs were used in this study: (1) smooth PTFE ball–smooth PDMS disc, (2) smooth PTFE ball–rough PDMS disc, (3) smooth PDMS ball–smooth PDMS disc, and (4) smooth PDMS ball–rough PDMS disc. The smooth PTFE balls were donated by Hoover Precision Products (Sault Ste Marie, Michigan, USA) and smooth PDMS balls were supplied by PCS instruments (London, United Kingdom). The PDMS discs were fabricated from a two-component silicone elastomer kit, Sylgard 184 (Dow Corning, Midland, Michigan, USA). The elastomer base and curing agent were combined in a ratio of 10 : 1 by mass and 3.2 mm thick sheets were cast in vertical aluminium–glass moulds. Smooth PDMS discs were produced by casting against the glass plate and rough discs were cast against a sandblasted aluminium plate. The PDMS sheets were cured in an 80 °C oven for approximately 4 hours. After cooling, the PDMS sheets were removed from the moulds and discs (D = 48 mm) were cut from the sheets. The r.m.s. surface roughness of the surfaces were characterised using a stylus profilometer (Dektak 150, Veeco, New York) and are presented in Table 1.

3.2. Lubricant systems

Three lubricant series were tested in this study: (1) glycerol–water-mixtures, ranging from 0 to 60% glycerol (ChemSupply); (2) glycerol–ethanol–water mixtures comprising 10% glycerol and ethanol concentrations ranging from 30% to 90%; (3) glycerol–ethanol–water mixtures comprising 40% glycerol and ethanol concentrations ranging from 20% to 60%. The densities and dynamic viscosities of these Newtonian fluids at 35 °C are given in Table 2. Viscosities were determined using size 50 and 100 series Canon-Fenske glass capillary viscometers (Cannon Instrument Company, State College, Pennsylvania, USA) in a temperature-controlled water bath. The two ternary glycerol–ethanol–water series were constructed in order to maintain a relatively constant viscosity while varying the surface tension. The ternary lubricant series containing 10% and 40% glycerol have viscosities of 1.8 ± 0.3 and 4.6 ± 0.3 mPa s, respectively.

3.3. Tribological measurement

The tribological properties of all lubricant systems were characterised using a ball-on-disc tribometer (MTM2, PCS Instruments Ltd, London, United Kingdom) fitted with compliant contacts. The friction force F_f was measured as a function of the entrainment speed, U, defined as the average surface speed of the ball and disc, $U = (U_{ball} + U_{disc})/2$, over the range of 1 to 3000 mm s^{-1} in logarithmic intervals. Measurements were carried out for six repetitions of alternately descending and ascending entrainment speed. For all tests, a normal load (W) of 2 N was applied on the ball and a SRR of 50% was used to impart both sliding and rolling motion, where SRR = $|U_{ball} - U_{disc}|/U$. The friction coefficient (μ) is calculated as the friction force divided by applied load ($\mu = F_f/W$). According to Hertzian contact mechanics, the PTFE–PDMS and PDMS–PDMS tribo-contacts under the load tested would have indentation depths of approximately 180 μm and 389 μm, and apparent contact radii of 1.30 mm and 1.90 mm, respectively (calculations provided in the ESI†).

Table 1 Surface roughness of tribo-surfaces, measured using a stylus profilometer

Tribo-surface	Surface roughness (r.m.s)
Smooth PTFE ball	41 ± 8 nm
Smooth PDMS ball	18 ± 3 nm
Smooth PDMS disc	39 ± 7 nm
Rough PDMS disc	5.2 ± 0.6 μm

Table 2 Densities and viscosities for the binary glycerol–water and ternary glycerol–ethanol–water lubricant systems

Glycerol conc. (wt%)	Ethanol conc. (wt%)	Density at 35 °C (g mL^{-1})	Dynamic viscosity at 35 °C (mPa s)
0	0	0.99	0.73
10	0	1.02	0.91
20	0	1.05	1.20
25	0	1.06	1.40
30	0	1.08	1.64
35	0	1.09	1.93
40	0	1.10	2.30
45	0	1.11	2.89
50	0	1.12	3.57
55	0	1.14	4.68
60	0	1.15	6.01
10	30	0.97	1.93
10	45	0.93	2.07
10	60	0.89	1.98
10	75	0.85	1.70
10	90	0.80	1.28
40	20	1.06	4.11
40	30	1.02	4.60
40	40	0.98	4.80
40	50	0.96	4.78
40	60	0.95	4.52

The lubricants were maintained at the desired test temperature of 35 °C (to reflect a typical biological system) using a silicone oil temperature bath (DC30-K20, Haake) and samples were pre-heated in a circulatory water bath. Prior to testing, the PDMS contacts were cleaned by gently rubbing the surface with a lens-cleaning wipe soaked in 1% SDS solution. They were then ultra-sonicated in 1% SDS solution, followed by thorough rinsing and ultra-sonication in RO water to remove all surfactant molecules.

At low entrainment speeds, the load and SRR can become unstable as a result of stick-slip behaviour arising from relatively strong adhesion between tribo-surfaces. Hence, all tribological data is filtered to eliminate data points that do not satisfy the following tolerances: 45% < SRR < 55% and 1.9 < W < 2.1 N. The Stribeck curve for each lubricant is fitted with an empirical model in eqn (1), as defined by Bongaerts *et al.*:[10]

$$\mu_{total} = \mu_{EHL} + \left(\frac{\mu_b - \mu_{EHL}}{1 + \left(\frac{U\eta}{B} \right)^m} \right) \quad (1)$$

where $\mu_{EHL} = k(U\eta)^n$ and $\mu_b = h(U\eta)^l$.

3.4. Contact angle measurement

The macroscopic static contact angles of all glycerol–water and glycerol–ethanol–water systems were characterised in air on rough and smooth PDMS substrates using an OCA20 contact angle goniometer (Data Physics Corporation, San Jose, California, USA). Still images of 10 μL droplets were taken after a contact time of 10 and 60 seconds and analysed according to the Pendant drop method, using the SCA20 software. There was no significant change in contact angle between the two measurement times. The contact angles of eight droplets were determined for each lubricant–substrate combination and averaged. All contact angle measurements were performed at ambient temperature (approximately 23 °C) since no temperature control was available. The discrepancy in temperature between the tribological and contact angle measurements is considered to have minimal impact since contact angle only has a weak dependence on temperature[26].

4. Results and discussion

The results and associated discussion is divided into five subsections: the first section presents the general shape of the Stribeck curve for the various tribo-systems and discusses the governing friction mechanisms based on the theory. The second section focuses on the effect of lubricant viscosity on lubrication for the glycerol–water mixtures with similar static wetting properties. The third section describes the distinct mechanisms by which lubricant viscosity impacts lubrication in smooth *versus* rough contacts. The fourth section uses glycerol–ethanol–water mixtures to assess the influence of static wetting on lubrication, independently of viscosity. Finally, a conceptual model is presented to summarise and explain the observed behaviour.

4.1. General shape of the Stribeck curve

Fig. 2 shows the friction coefficient as a function of entrainment velocity for a PTFE ball in tribological contact with (A) a smooth and (B) a rough PDMS disc. The corresponding data obtained using a PDMS ball in contact with the same counter-surfaces are presented in ESI,† Fig. S1 for reference; however, the analysis and interpretation is better demonstrated using the PTFE–PDMS data. The same general trend in tribological data is observed for all tribo-pairs and across the range of lubricant systems – the friction coefficient increases logarithmically with entrainment velocity up to a critical velocity, beyond which it decreases. (Note: this initial logarithmic increase is not captured well for the smooth PDMS–PDMS tribo-pair due to low speed instabilities arising from high adhesion and subsequent truncation of data.) At very high entrainment velocities, a minimum in the friction coefficient is observed for the highest viscosity fluids in the smooth contact (visible on a log–log plot). This characteristic shape is predicted by Scaraggi and Persson's theoretical model[17] and can be explained in terms of the dissipation mechanisms at play in the tribological contact. Fig. 3 and Fig. S2 (ESI†) show the same friction coefficient data as in Fig. 2 and Fig. S1 (ESI†), respectively, plotted as a function of the reduced velocity, $U\eta$. The rubber-to-glassy transition regions of the

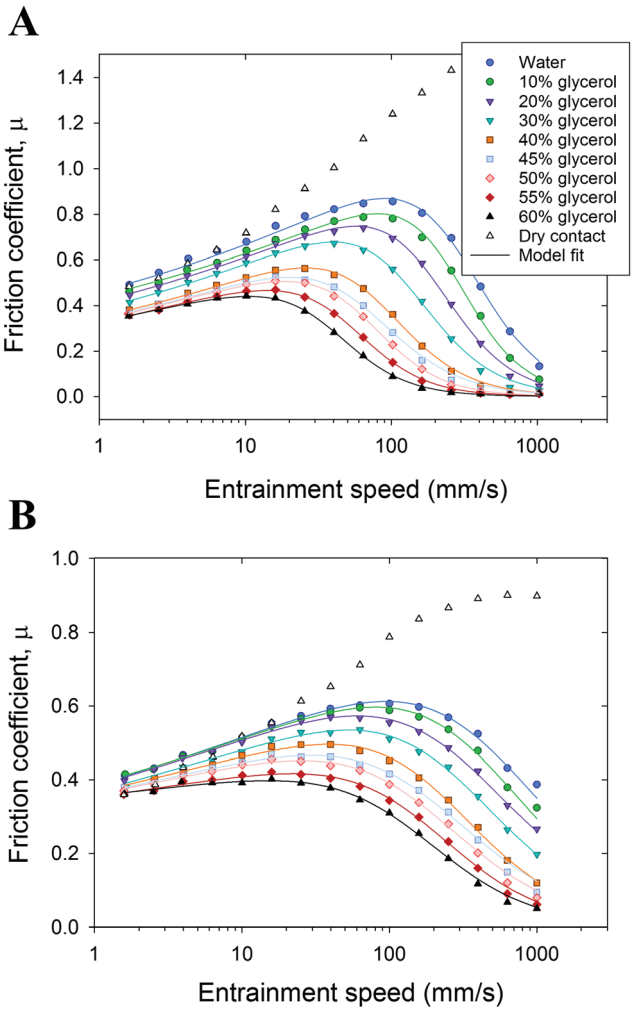

Fig. 2 The friction coefficient as a function of entrainment velocity for the series of glycerol–water mixtures, as well as the dry contact, for a PTFE ball in tribological contact with (A) a smooth and (B) a rough PDMS disc. The friction curves for all lubricants exhibit a characteristic shape, which is predicted by theoretical models and explained in terms of viscoelastic dissipation mechanisms.

Stribeck curve, as defined in their model, are more clearly observed in this format, as labelled for the PFTE–PDMS tribo-pair in Fig. 3A and B. The tribological profiles are fitted with empirical eqn (1) and the corresponding model parameters, which characterise the unique shape of each curve, are discussed in Section 4.3 in terms of viscosity and roughness effects. It was not possible to generate good model fits for the smooth PDMS–PDMS contact due to the lack of stable measurements in the rubbery region arising from the self-adhesive nature of the PDMS. Hence, the focus of the analysis is on the remaining three (less adhesive) tribo-pairs.

Below the critical velocity, the friction force for all lubricants is shown to increase logarithmically with velocity, which is consistent with an activated molecular relaxation process occurring in the PDMS[27] *i.e.* the viscoelastic substrate is in a rubbery state. Based on Scaraggi and Persson's[17] theoretical model, the characteristic peak in friction coefficient observed for all lubricant systems is

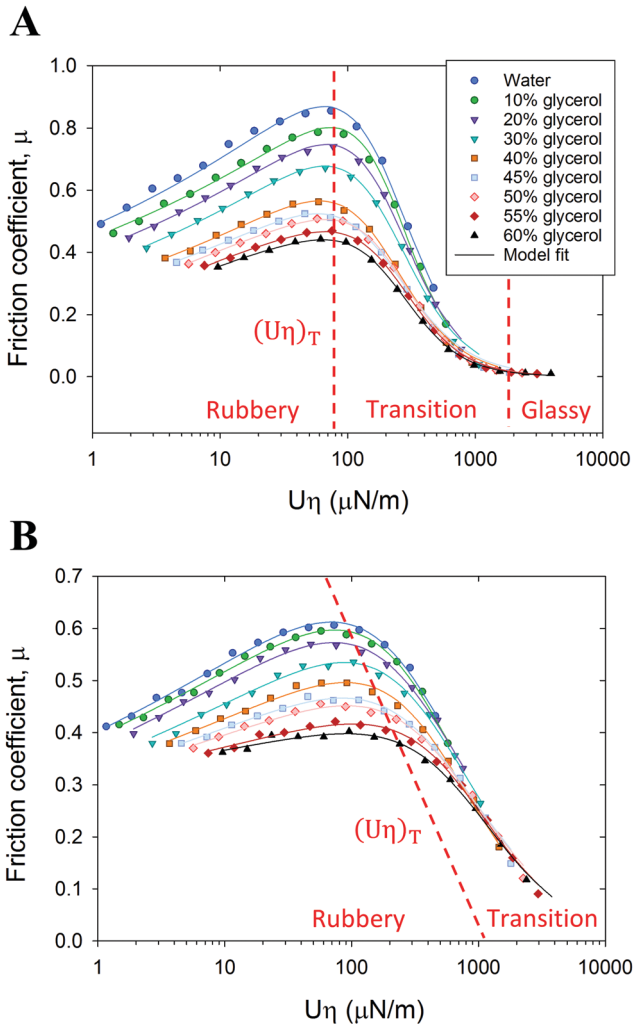

Fig. 3 The same friction data as in Fig. 2, for the series of glycerol–water mixtures, plotted as a function of reduced velocity, $U\eta$ (entrainment speed multiplied by lubricant viscosity) for (A) a smooth and (B) a rough PTFE–PDMS contact. Different regions of the Stribeck curve, defined by the transition from a rubbery to glassy response of the viscoelastic PDMS, are observed and indicated by the dotted lines.

governed by the solid-contact rolling friction and represents the competition between the characteristic time-scale of the tribological process (*i.e.* the loading and unloading time) *versus* the relaxation time of the PDMS. For dry contacts, the maximum dissipation (and rolling friction) occurs when the time of loading/unloading coincides with the relaxation time of the material.[24] Beyond this critical velocity, the internal relaxation of the PDMS is slower than the loading/unloading time, leading to a decrease in viscoelastic dissipation (solid-contact rolling friction) and marking the onset of the transition region. This time-scale imbalance is also predicted to lead to an increase in the effective elastic modulus of the PDMS with increasing velocity, and subsequently, a reduction in contact area and solid-contact sliding friction. It should be noted that, for the lubricated contacts studied here, the critical velocity corresponding to the peak in friction can also be affected by fluid–asperity interactions (wet-rolling friction), especially at higher lubricant viscosities. This is discussed in more detail in the following sections. At even higher reduced velocities, the tribological time-scale is much faster than the relaxation time and the deformation of PDMS is primarily elastic *i.e.* in a glassy state. The glassy region is observed here only for the smooth contact, as labelled in Fig. 3A.

An important point should be emphasised here with regards to defining and labelling lubrication regimes. The decrease in friction coefficient beyond the critical velocity, observed here for all lubricants, is commonly considered to indicate the onset of the mixed lubrication regime; that is, the transition from an asperity-dominated contact to one that is dominated by fluid hydrodynamics. However, the model of Scaraggi and Persson[17] highlights that the 'true' transition point between the boundary, mixed and hydrodynamic regimes for viscoelastic contacts does not necessarily coincide with the minima and maxima in the Stribeck curve. This decrease in friction can equally occur due to a 'stiffening' of the contact due to the competing time-scales described above. This interpretation is contrary to many experimental studies in the field, since they were developed from more traditional tribological studies involving harder substrates. The inability to easily define the transitions in viscoelastic contacts suggests that theoretical and numerical modelling play a crucial role in developing an enhanced mechanistic understanding of the underlying dissipation processes, which can then be applied to more accurately interpret experimental data, as exemplified in this paper.

Friction data for the dry contacts are also included in Fig. 2 and Fig. S1 (ESI†). For the smooth contact (Fig. 2A and Fig. S1A, ESI†), the friction coefficient monotonically increases with entrainment speed for the range tested, whereas an apparent plateau or maximum is observed for the rough PTFE–PDMS contact (Fig. 2B). It is anticipated that for higher velocities (beyond the current measurement limitations), a decrease in friction coefficient would also be observed for the dry contacts; this is supported by dry elastomeric friction studies that show a destabilisation beyond a critical velocity when stick-slip sliding occurs and the contact area shrinks from adhesive (JKR) to Hertzian.[28]

Also interesting is that, for the rough contact, the wet-lubricated contact generates higher friction than the dry contact at low entrainment speeds, whereas in the smooth case, the dry friction is higher than or equivalent to the friction generated by the lowest viscosity lubricant (water). This is observed for both PTFE–PDMS and PDMS–PDMS tribo-pairs and suggests that there may also be capillary-driven adhesion or some other fluid effect within the asperities of the rough contacts acting to increase the friction coefficient. We will return to this point in Section 4.3.

4.2. Influence of lubricant viscosity

It is immediately clear in Fig. 3 and Fig. S2 (ESI†) that, for both smooth and rough tribo-pairs, there is no collapse of the data onto a single Stribeck master curve, as may typically be anticipated after scaling with viscosity. Instead, the friction coefficient decreases with increasing viscosity over a wide range of $U\eta$ values. It is also observed for the PTFE–PDMS tribo-pair

that the Stribeck curves generated for the smooth contact maintain a similar shape as a function of viscosity, whereas a loss of vertical symmetry in the friction curve is seen for the rough contact. This roughness effect is discussed in detail in Section 4.3. (Again, it is difficult to observe these differences in symmetry for the PDMS–PDMS tribo-pair due to the truncation of data at low speeds.) The differentiation between the tribological profiles of various Newtonian lubricants indicates that fluid viscosity has an impact on lubrication beyond its direct contribution to wet-contact sliding friction (Couette and Poiseuille friction). Therefore, in order to interpret the data presented here it is necessary to consider the effect of viscosity on the remaining three identified components of friction: solid-contact rolling, wet-contact rolling, and solid-contact sliding friction.

Solid-contact rolling friction at the macro-scale represents the viscoelastic hysteresis losses induced by bulk deformation of the PDMS elastomer in contact with the counter-surface, hence lubricant viscosity is not anticipated to have a direct effect on this component of friction. At the asperity-scale, however, viscoelastic dissipation arising from asperity deformation is expected to be a function of lubricant viscosity, whereby the trapped fluid provides viscous damping and subsequently increases the relaxation time of the asperities. This effect impacts the competition between the asperity relaxation time and the tribological strain rate and hence the solid-contact rolling friction profile. However, the contribution of asperity deformation losses to the overall solid-contact rolling friction is likely to be minimal compared to losses arising from macroscopic deformation since the Hertzian indentation depth is much larger than the surface roughness (asperity height) for all tribo-contacts.

Wet-contact rolling friction arises from a combination of fluid viscous losses and viscoelastic deformation losses induced by fluid pressure asymmetry acting on the PDMS. According to Scaraggi and Persson's model,[17] the relative contribution of the latter increases with lubricant viscosity and has the greatest impact on the Stribeck curve in the mixed lubrication transition range of velocities, during which the transfer of normal load from the asperity contacts to the fluid stimulates fluid-induced viscoelastic hysteresis of the PDMS. Furthermore, as the lubricant viscosity increases, the wet- and solid-contact rolling friction components coincide and the fluid pressure field is affected by the rubbery-to-glassy transition of the PDMS. This fluid viscosity effect has an impact on the overall shape of the Stribeck curve for rough *versus* smooth contacts (discussed in Section 4.3), but does not explain the decrease in friction with increasing viscosity observed here.

Thus, we now consider the effect of lubricant viscosity on solid-contact sliding friction, which represents the viscoelastic dissipation of interfacial elastomer molecules during adhesive bonding and debonding events between the two solid substrates. This mechanism is described in literature for dry elastomeric friction.[28] Interfacial adhesion arises from interdiffusion, interpenetration and entanglement of chains across the polymer–polymer contact interface and thus requires a degree of chain mobility.[29] We hypothesise that increasing the viscosity of the confined fluid film (if present) influences this molecular motion. Hydrodynamic theory for single-molecules predicts that an increase in lubricant viscosity corresponds to a slower relaxation time of the interfacial PDMS molecules[30,31] and deeper potential energy wells exist which restrict molecular motion and less adhesive bonds are able to form. In other words, for a given sliding velocity (or loading/contact time), the elastomer molecules are less effective in facilitating interfacial adhesion; hence, interfacial shear stress and friction decrease with increasing lubricant viscosity, as observed in Fig. 3 and Fig. S2 (ESI†). The increased fluid pressure and hence film thickness generated by a higher viscosity lubricant is expected to further hinder adhesive bond formation. Weaker interfacial interactions also lead to a reduction in bulk deformation and thus solid-contact rolling friction could be indirectly influenced by lubricant viscosity. We propose this as a possible mechanism of friction reduction to (partially) explain the lubrication enhancement for higher lubricant viscosities.

Finally, we must consider the influence of fluid viscosity on the dewetting and squeeze-out dynamics of the lubricant in the tribo-contact, since these effects determine the degree of fluid entrainment, and hence the relative contribution of wet- *versus* solid-contact friction components as a function of entrainment speed. Fluid squeeze-out dynamics relates to the rate of fluid removal from the asperity contact regions and is governed by global flow of fluid at the tribo-interface, whereas dewetting transitions involve the (thermally activated) nucleation of localised dry contact regions originating near the top of the asperity contacts when the film thickness becomes small enough.[32] Both processes result in a time-dependent increase in the real area of contact and hence an increase in the solid-contact friction. We propose that the combined effects of squeeze-out and dewetting contribute considerably to the observed decrease in friction coefficient with increasing lubricant viscosity shown in Fig. 3 and Fig. S2 (ESI†).

In Fig. 5, the static contact angles (θ_s) of the binary glycerol–water solutions on PDMS are shown to be independent of glycerol concentration, and hence viscosity, for both smooth and rough substrates, which suggests that glycerol molecules do not have a strong association with the PDMS surface. However, under dynamic conditions, such as those in a tribological contact, wetting behaviour is known to be a function of viscosity, where higher viscosity fluids exhibit greater contact angle hysteresis and hence lower receding contact angles,[33] an important parameter governing dewetting behaviour. The dependence of dynamic contact angle on fluid viscosity also increases with sliding velocity, as reported for glycerol–water systems.[34] Furthermore, the squeeze-out rate of fluid from the asperity contact regions also decreases with increasing fluid viscosity.

Therefore, the friction force generated at each value of entrainment speed depends on the rate of lubricant squeeze-out and dewetting of the contact *versus* the time-scale of the shearing motion which serves to drag fluid between the ball and disc, thus replenishing the contact zone. As the sliding (and entrainment) speed decreases, the fluid has more time to be squeezed out and dewet the nominal contact area; hence,

the lower viscosity lubricants such as water undergo a higher degree of fluid removal, resulting in higher solid-contact friction, as observed in Fig. 3 and Fig. S2 (ESI†). In other words, the local dewetting transition velocities decrease as lubricant viscosity increases, meaning that the lubricant is excluded from an increasing number of local asperity contacts at a higher velocity for low viscosity lubricants. Conversely, the higher viscosity lubricants (higher glycerol concentration) inhibit squeeze-out and dewetting, even at very low entrainment speeds, thus reducing the solid-contact friction. In addition, deformation of the PDMS surface between asperities by the fluid pressure would further reduce the fluid squeeze-out rate for higher viscosity fluids. The squeeze-out and dewetting effects described here hold for both the rough and smooth contacts, since the smooth surfaces used in this study are not molecularly smooth.

In consideration of the aforementioned multi-scale viscoelastic and wetting effects, we attribute the decrease in friction coefficient with increasing viscosity observed here for all tribo-pairs to the effect of lubricant viscosity on:

(1) dewetting and squeeze out-dynamics, and

(2) the (interfacial) adhesion and viscoelastic dissipation of interfacial elastomer molecules in bonding and debonding events.

The reduction in the friction coefficient with increasing viscosity represents a notable deviation from Scaraggi and Persson's theoretical model. In particular, the effect of viscosity on friction at very low values of $U\eta$ suggests that fluid is still present in the contact even at very low entrainment speeds, contrary to Scaraggi and Persson's model predictions for similar viscosities. This is considered to arise primarily from the lack of existing physical models to simultaneously describe the squeeze-out and collective dynamics of dewetting asperities for randomly rough (non-molecularly smooth) surfaces. Also, the dependence of dewetting speed on the viscoelastic hysteresis was not included in deriving their model.[17] The discrepancy between the experimental data presented here and the theoretical predictions and may also be partially ascribed to their model assumption that the solid-contact shear stress is independent of the lubricant viscosity, which discounts the potential effect of fluid viscosity on interfacial adhesion mentioned here. Advances in theoretical and numerical modelling combined with further experimental studies will provide more insight into the relative contribution of these viscosity effects.

4.3. Influence of roughness on viscosity effects

Now that we have established the key physical mechanisms governing the friction behaviour of the lubricated tribo-systems studied here, we focus on the key differences in the dynamics of the smooth *versus* rough contacts. A comparison of Fig. 3A and B highlights that, in the smooth case, the same general shape in the Stribeck curve is maintained as a function of viscosity, whereas for the rough contact, the friction peak flattens with increasing viscosity and there is a loss of symmetry in the data as compared to the smooth surface. Some of these differences may be subtle in a visual context, however, upon extraction of some key parameters from data fitting, we are able to observe clear systematic changes in the shape of the friction profiles. Fig. 4 shows three of these parameters as a function of lubricant viscosity for the smooth and rough PTFE–PDMS contact, as well as the rough PDMS–PDMS contact: (A) the maximum friction coefficient, μ_{max} (B) the logarithmic slope of the rubbery region and (C) the reduced velocity at the transition from the rubbery to transition regime, $(v\eta)_T$. There are several key differences in the tribological profiles generated using the smooth *versus* rough PDMS disc, which provide some insight into the dissipation mechanisms that dominate the friction produced in each case.

Firstly, the peak friction values are lower in the case of the rough compared to smooth PTFE–PDMS contact for all viscosities tested, although there is less discrepancy at high viscosities, as shown in Fig. 4A. The rate of decrease in peak friction with increasing viscosity is also higher for the smooth surface. The reduction in friction with increasing roughness is considered to be the net result of several competing effects. Firstly, the solid-contact sliding friction is expected to decrease with increasing surface roughness due to a reduction in the real area of contact available for interfacial interaction between the two solid surfaces. A further decrease in the solid-contact rolling friction for the rough contact arises from the increase in the apparent contact area (due to surface irregularities) which results in a reduction in nominal contact pressure and indentation depth. Although, this reduction in bulk deformation is counteracted by additional contributions to the solid-contact rolling friction from asperity deformation. In the smooth case, however, stronger interfacial interactions are anticipated to drive additional bulk deformation and contribute to the higher measured friction, compared to the rough contact. Finally, the fluid squeeze-out rate is higher for the rough contact since large percolation channels provide a means for fluid to rapidly escape to the edge of the nominal contact area, whereas for a smooth contact, fluid can become confined and trapped within local cavities, considerably reducing the squeeze-out speed and hence solid-contact friction.[32] This effect leads to a relative increase in friction for the rough compared to smooth contact, which contradicts the trend observed here, suggesting that it is not the dominant mechanism. It does, however, offer a possible explanation for the convergence of peak friction values for the smooth and rough contact at high lubricant viscosities, where the dependence of squeeze-out on roughness would be more pronounced. Note that friction generated by the interlocking of opposing asperities is expected to be minimal in this case, since the ball roughness is much smaller than the disc roughness. However, a comparison between a 'rough ball on rough disc' and 'smooth ball on smooth disc' may yield considerably different results due to the potential for 'interlocking friction' between two rough surfaces.

The higher maximum friction generated for the rough PDMS–PDMS compared to the rough PTFE–PDMS contact (Fig. 4A) can be explained in terms the higher interfacial friction per unit area resulting from the strong self-adhesive nature of PDMS. Additionally, the two-fold larger Hertzian indentation depth and contact area of the PDMS–PDMS tribo-pair, arising from

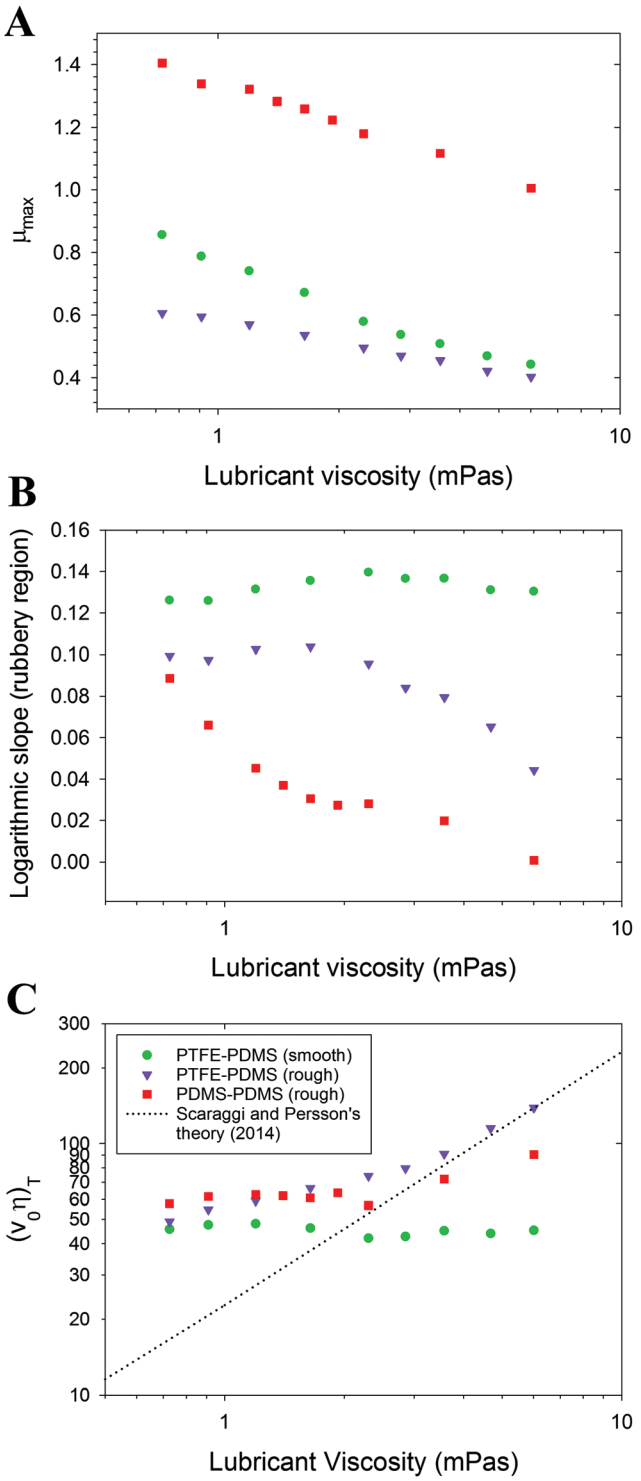

Fig. 4 Model parameters that define distinguishing features the Stribeck curves, plotted as a function of lubricant viscosity: (A) peak friction coefficient; (B) logarithmic slope of the rubber region; (C) critical reduced (sliding) velocity, corresponding to the junction between the rubbery and transition regime. Key differences in the tribological profiles generated using the smooth *versus* rough PDMS disc are highlighted, and provide insights into the governing dissipation mechanisms and the related role of viscosity.

the use of two highly compliant substrates, result in additional rubber deformation and solid-contact sliding friction.

Fig. 4B shows that the slope of the rubbery region decreases with increasing viscosity for rough surfaces, whereas it is relatively constant for smooth surfaces. This is attributed to the differences in squeeze-out and dewetting dynamics for smooth *versus* rough contacts. As mentioned above, for the rough contact, squeeze-out and dewetting occurs more rapidly and the lubricant is increasingly expelled from the contact as the tribological time-scale increases (entrainment speed decreases). At the lowest measured entrainment speed, the fluid is almost completely removed and the friction coefficient for all lubricant viscosity systems converges to the same value *i.e.* the dry friction coefficient, as illustrated in Fig. 2B, thus explaining the decrease in the slope of this region with increasing viscosity. However, for the smooth contact, the squeeze-out and dewetting is much slower and results in confined (sealed-off) fluid regions, which further impedes the squeeze-out; hence, fluid remains trapped in the contact and the friction coefficient is lower for higher viscosity lubricants, even at the lowest measurable entrainment speed. It is expected that if we were to measure beyond the current limitations of the tribometer to lower speeds, the data for the smooth contact would also approach (but may not reach) the dry friction curve.

These squeeze-out and dewetting effects also explain why rough contacts have greater friction than smooth at low entrainment speeds (<10 μN m^{-1}), as observed in Fig. 3. Furthermore, the value of reduced velocity at which the friction generated in the rough contact surpasses the smooth contact friction (for the same lubricant) increases with fluid viscosity, from 1 to 10 μN m^{-1} for viscosities of 1.2 and 6.0 mPa s, respectively.

It is also observed in Fig. 3 that the maximum in the friction coefficient occurs at a higher velocity for the rough compared to the smooth surface – a trend reported previously for dry viscoelastic contacts.[35] However, this trend is also supported by Scaraggi and Persson's model for wet contacts, which predicts that the critical velocity corresponding to the maximum in the solid-contact rolling friction (v_T) occurs when $v_T \approx a_0/\tau_r$ (*i.e.* the Hertzian contact radius divided by the rubber relaxation time). Since the width of the apparent contact area increases with surface roughness, the critical velocity is also expected to increase with roughness. More interestingly, however, are the differences in the friction profiles as a function of viscosity.

Fig. 4C shows the reduced velocity at the transition from the rubbery to the transition regime, $(v\eta)_T$, calculated by determining the intersection of the two logarithmic curves fitted to the data for each regime, as a function of viscosity. For the sake of comparison with the critical reduced velocities predicted by Scaraggi and Persson's model, we use the product of the lubricant viscosity and the sliding speed, v (rather than entrainment speed, U). For the smooth PTFE case, the transition velocity remains constant with lubricant viscosity; however, for both rough contacts (PTFE and PDMS) there is a shift in the critical reduced velocity to higher $v\eta$ values with increasing fluid viscosity. This is also illustrated in Fig. 3B, where the dotted line shows the onset of the transition region, which increases with lubricant viscosity.

The shift in $(v\eta)_T$, to higher values as viscosity increases for rough, but not smooth, surfaces can be explained in terms of the asperity-scale viscoelastic effects described in Section 4.2.

The transfer of normal load from the asperity contacts to the fluid pooled between asperities increases the locally averaged fluid pressure, which results in the PDMS substrate being hysteretically stimulated by the fluid–asperity interactions *i.e.* wet-rolling friction. Both the wet-contact rolling and wet-contact sliding friction are present at much lower reduced velocities in the rough compared to the smooth contact due to the availability of fluid between the asperities. That is, for rough soft contacts, the viscoelastic region (and the maximum in the loss tangent) coincides with the mixed lubrication transition range of velocities. This affects the shape of the resulting Stribeck curve, which is formed by the summation of these components, as illustrated in Fig. 1B. This is exemplified in Fig. 3 and 4C where we observe a flattening of the friction peak and a shift to higher reduced velocities for the rough contact, in contrast to the symmetry in the data for the smooth contact.

This trend is in alignment with the model predictions reported by Scaraggi and Persson[17] for a rough, viscoelastic contact. The dotted line in Fig. 4C shows the critical reduced velocities predicted by Scaraggi and Persson's model, which are also shown to increase with lubricant viscosity and are in good agreement with the values for both rough contacts for viscosities above around 2 mPa s. However, the theoretical model deviates from the experimental data at lower lubricant viscosities; experimentally, the dependence of the critical reduced velocity on the lubricant viscosity weakens (*i.e.* decreasing slope) at low fluid viscosities. The discrepancy between the model predictions and experimental data presented here is attributed to the absence of theory and modelling to describe the dewetting and squeeze-out dynamics for randomly rough contacts, as well as model assumptions regarding substrate properties (*e.g.* multiscale roughness, viscoelastic properties), which deviate from those used in this experimental study.

4.4. Separating viscosity and wetting effects

As we have already discussed, lubricant viscosity impacts the dynamic wetting, de-wetting and squeeze-out dynamics and these effects play an important role is viscoelastic lubrication. In this section, we attempt to isolate the effects of lubricant viscosity *versus* the lubricant's equilibrium adhesive interaction with the solid substrates (static wetting). This is investigated using two sets of ternary glycerol–ethanol–water systems, which are formulated such that variations in ethanol concentration modulate the surface tension, while constant glycerol concentrations maintain relatively constant viscosities of 1.8 ± 0.3 and 4.6 ± 0.3 mPa s across the two lubricant series (referred to herein as the 'low' and 'high' viscosity ternary series, respectively).

Fig. 5 shows the measured static contact angles, θ_s, as a function of glycerol concentration for glycerol–water systems (upper *x*-axis) and ethanol concentration for glycerol–ethanol–water systems (lower *x*-axis). The static contact angle is shown to be independent of glycerol concentration for both the binary and ternary systems, on smooth and rough PDMS substrates. For the ternary systems, the contact angle is a function of the ethanol concentration only, since it follows the same linear dependence at both 10% and 40% glycerol. Higher concentrations of ethanol act to lower the surface tension of the ternary

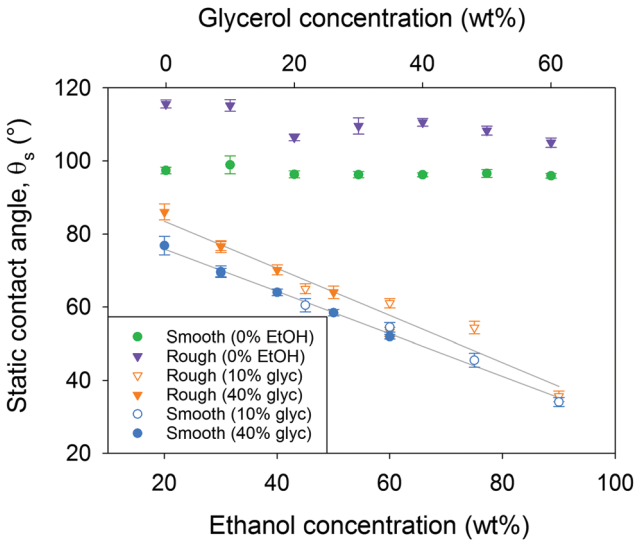

Fig. 5 Static contact angles as a function of glycerol concentration for the binary glycerol–water systems (upper *x*-axis) and ethanol concentration for ternary glycerol–ethanol–water systems (lower *x*-axis). For the ternary systems, the glycerol concentration is indicated by open symbols (10% glycerol, low viscosity) and closed symbols (40% glycerol, high viscosity).

system and enhance surface wetting, thus reducing the contact angle. The slope of the data is constant for the smooth and rough case, suggesting that there is no Cassie impregnation on the rough surface, or at least that this is not a function of surface tension. The contact angle of all lubricants is higher on the rough PDMS substrate compared to the smooth surface, as expected for a hydrophobic material based on the Wenzel or Cassie–Baxter state of wetting.

The Stribeck curves for the low and high viscosity ternary lubricant series are presented in ESI,† Fig. S3 and S4, respectively. In each case, the raw data (μ as a function of U) and the scaled data (μ as a function of $U\eta$) are shown for both smooth (A and B) and rough (C and D) PDMS–PDMS contacts. The full friction profiles are presented as ESI,† since the discussion here focusses on the key parameters that describe these curves: the peak friction coefficient, μ_{max} (Fig. 6) and the transition reduced velocity, $(U\eta)_T$ (Fig. 7).

Fig. 6 shows μ_{max} as a function of θ_s for all ternary lubricant systems. The peak friction coefficient is shown to decrease as the static contact angle decreases for both the low and high viscosity lubricant series on smooth and rough PDMS–PDMS contacts, attributed to the increase in spreading rate and fluid-film formation within the contact zone. More interestingly, the higher viscosity lubricant series generates consistently lower peak friction coefficients compared to the low viscosity series for equivalent static contact angle values. This finding supports the hypothesis that viscoelastic lubrication is governed both by the equilibrium wetting properties and viscosity-driven dynamic dewetting and squeeze-out dynamics. That is, the process of dewetting and squeeze-out from the contact zone is slower for higher viscosity lubricants, resulting in reduced solid-contact friction.

Fig. 7 shows $(U\eta)_T$ as a function of θ_s for the low and high viscosity ternary series in rough PDMS–PDMS contacts.

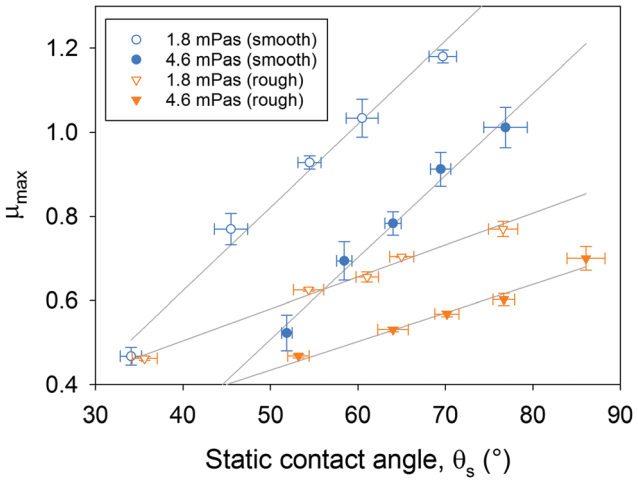

Fig. 6 Peak friction coefficient, μ_{max}, as a function of the static contact angle, θ_s, for all ternary lubricant systems in smooth and rough PDMS–PDMS contacts.

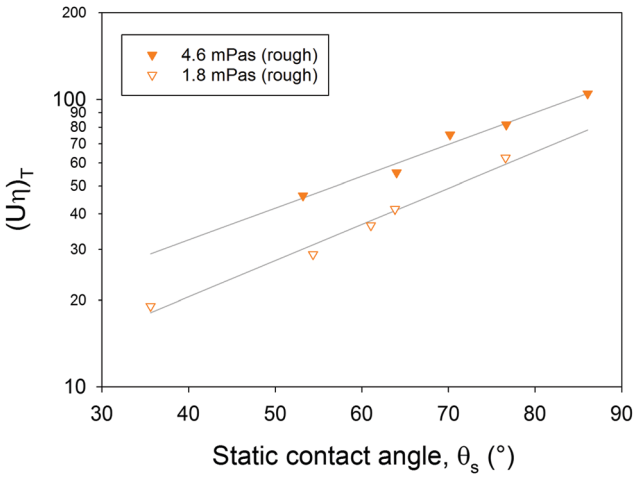

Fig. 7 The transition reduced velocity, $(U\eta)_T$, as a function of the static contact angle for the low and high viscosity ternary series in rough PDMS–PDMS contacts.

$(U\eta)_T$ was calculated in the same way as previously, by determining the intersection of the logarithmic curves fitted to the data for the two regimes. It was not possible to accurately identify these transition points for the smooth contact since the transition occurs at lower reduced velocities where measurement instabilities occur. $(U\eta)_T$ is shown to increase linearly with lubricant θ_s for both viscosity series within the rough contact. While the slope is constant for both viscosity series, the data for the higher lubricant viscosity is shifted to higher values of $(U\eta)_T$ at equivalent contact angles. This indicates that both the lubricant viscosity and equilibrium wetting adhesion affect the transition from the rubbery to the transition state. The latter is explained by the fact that, as the wetting adhesion increases (contact angle decreases), the lubricant is more readily dragged and entrained into the contact zone, hence the onset of wet-contact friction and reduction in solid-contact sliding friction occurs at lower values of $U\eta$. Lubricant viscosity also controls the degree of fluid entrainment, whereby higher viscosity lubricants are more resistant to squeeze-out and dewetting occurs at a slower rate, hence fluid is maintained in the contact down to much lower reduced velocities, as detailed in the previous sections. This trapped high-viscosity fluid also stimulates additional viscoelastic hysteresis in the PDMS *via* the increase in fluid pressure generated between the asperities, which leads to an increase in wet-rolling friction with respect to solid-contact rolling friction and shifts $(U\eta)_T$ to higher values, as described by Scaraggi and Persson.[17]

The distinct mechanisms by which lubricant dewetting and squeeze-out occur in smooth *versus* rough contacts have already been described in Section 4.3. In this section, the same principles are applied to interpret the lubrication profiles generated for the two ternary lubricant series and hence elucidate the impact of surface roughness on the relative contribution of fluid dynamics (viscosity and dewetting) *versus* equilibrium interfacial energies (static wetting) to the overall friction profile.

In Fig. 6, the peak friction coefficient for the smooth contact shows a stronger dependence on the contact angle compared to the rough contact, evidenced by the higher slope in the data fit line. This is attributed to the slower rate of asperity dewetting in (non-molecularly) smooth *versus* rough contact discussed previously. In contrast to the rapid drainage of fluid from a rough contact, fluid entrained between smooth contacts is more likely to be trapped within the nominal contact area. Therefore, it is not surprising that fluid–solid interfacial interactions (wetting properties) have a stronger influence on the friction coefficient. Interestingly, the slope of the data is independent of the lubricant viscosity for both the smooth and rough contacts – the higher lubricant viscosity simply shifts the data to lower friction coefficient values.

The data for the smooth and rough contacts converge to similar peak friction values at low lubricant contact angle ($\sim 30^\circ$ for the low viscosity series and $\sim 45^\circ$ for the high viscosity lubricant series), suggesting that the surface roughness becomes less dominant as the lubricant contact angle decreases. This is because the roughness dictates the real area of contact and hence the solid-contact friction; this component of friction is dominant when the lubricant is removed from the contact zone in cases of low wettability (high contact angle). Note that the same convergence of smooth and rough data is seen for the binary glycerol–water systems at high values of viscosity and constant contact angle (Fig. 4A), reiterating that viscosity also plays a crucial role in squeeze-out dynamics. This is further supported by the fact that the convergence of rough and smooth data in Fig. 6 occurs at a higher contact angle for the higher viscosity lubricant series (45° compared to 30° for the low viscosity series). For the higher viscosity lubricants, squeeze-out dynamics are slower, which facilitates the retainment of fluid in the contact zone up to a higher lubricant contact angle and the roughness has less of an impact on the peak friction coefficient. Extrapolation of the linear fit lines would suggest that, for lubricants with even lower contact angle values, the rough contact would start to generate higher peak friction

values compared to the smooth contact (for equivalent contact angle and viscosity values). This is interpreted by considering the fact that surface roughness dictates both the real area of contact (solid-contact friction) and the rate of fluid removal from the nominal contact area. Since these two effects are directionally opposing, it is the relative contribution of each that determines the overall friction coefficient. Hence, it is proposed that the intersection of the data for the smooth and rough contacts represents the point at which the lubricant properties (viscosity and contact angle) provide a balance between these two competing roughness effects.

Further systematic experimental investigation, including dynamic wetting measurements, combined with theoretical and numerical modelling is required to isolate some of these effects and better elucidate the mechanisms that dominate over a range of conditions.

4.5. Multi-scale viscoelastic conceptual model

We propose a multi-scale viscoelastic conceptual model, illustrated in Fig. 8, to explain and summarise the observed lubrication behaviour and the role of fluid viscosity, wetting properties and surface roughness. This explanation is based on the coexistence of multiple viscoelastic lubrication mechanisms (labelled I, II, III and IV), which have traditionally been considered independently in the literature. However, it is proposed that the overall friction profiles of the lubricated systems studied here are determined by the complex interplay and competition between these four processes.

(I) On the macro-scale, viscoelastic hysteresis losses are induced by bulk deformation of the PDMS disc arising from the normal and shear forces applied by the counter-surface. Lubricant properties do not have a direct effect on this component of friction since it relates to the internal cohesion of the elastomer; however, the extent of bulk deformation is influenced by other friction mechanisms such as adhesion, and is therefore indirectly dependent on lubricant properties.

(II) At the asperity scale, fluid pressure asymmetry generated between asperities during the transfer of normal load from the asperity contacts to the fluid induces further viscoelastic hysteresis in the PDMS. Under certain lubricant conditions, these fluid–asperity interactions (wet-contact rolling friction) coincide with the bulk viscoelastic dissipation (solid-contact rolling friction), altering the overall shape of the Stribeck curve.

(III) At the sub-asperity scale, localised dewetting and squeeze-out dynamics control the degree of fluid removal from the nominal contact area and hence the relative contribution of wet-*versus* solid-contact friction over a range of tribological conditions. Dewetting and squeeze-out are in turn influenced by the viscosity and equilibrium wetting properties of the lubricant.

(IV) At a molecular level, interfacial friction arises from the formation of adhesive bonds between the two solid substrates, which become stretched under shear until they debond, relax and reattach, as shown in the schematic diagram. The viscosity of the confined fluid film (if present) governs this molecular motion and hence the solid-contact sliding friction arising from the viscoelastic dissipation of the interfacial elastomer molecules.

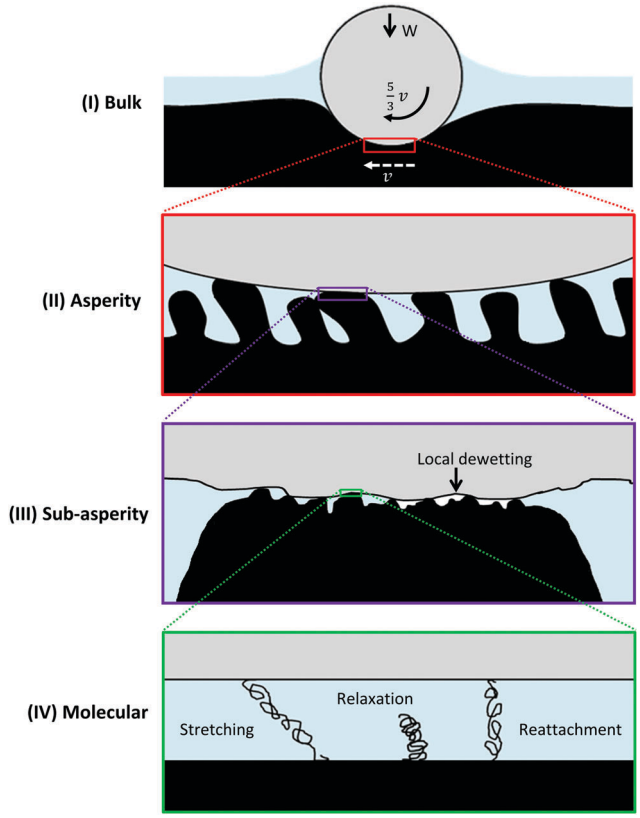

Fig. 8 The multi-scale viscoelastic conceptual model proposed to explain the influence of lubricant viscosity and static wetting on the tribological profiles of a smooth and rough contact. The schematic illustrates four key viscoelastic dissipation mechanisms operating at the macro-(bulk), asperity-, sub-asperity- and molecular-scale: (I) bulk viscoelastic deformation losses, (II) fluid-induced viscoelastic hysteresis, (III) localised dewetting and squeeze-out dynamics, and (IV) viscoelastic dissipation of interfacial elastomer molecules during bonding/debonding events.

The relative contribution of these four friction mechanisms is governed by the extent of fluid entrainment, as well as the static and dynamic properties of the lubricant (which also dictate the former). Fig. 9 illustrates the generalised trends in lubrication profiles as influenced by fluid viscosity and static wettability. For fluids with similar static wetting properties, increasing lubricant viscosity decreases the overall friction coefficient as a result of: (1) slower dewetting and squeeze-out of fluid which inhibits solid contact, (2) restricted molecular motion of interfacial elastomer molecules which reduces interfacial adhesion, and (3) reduced bulk deformation losses (solid-contact rolling friction) arising from (1) and (2). For fluids with similar viscosities, increasing their wettability (decreasing θ_s) also reduces solid-contact friction by promoting rapid spreading and perpetual fluid-film formation within the nominal contact area. For rough contacts, increasing lubricant viscosity also alters the overall shape of the friction profile by increasing the critical transition reduced velocity, $(U\eta)_T$, as a result of fluid-induced viscoelastic dissipation between asperities. In contrast, increasing wettability decreases $(U\eta)_T$ by enhancing the efficiency by which the fluid forms ultra-thin films that promote the onset of wet-contact friction.

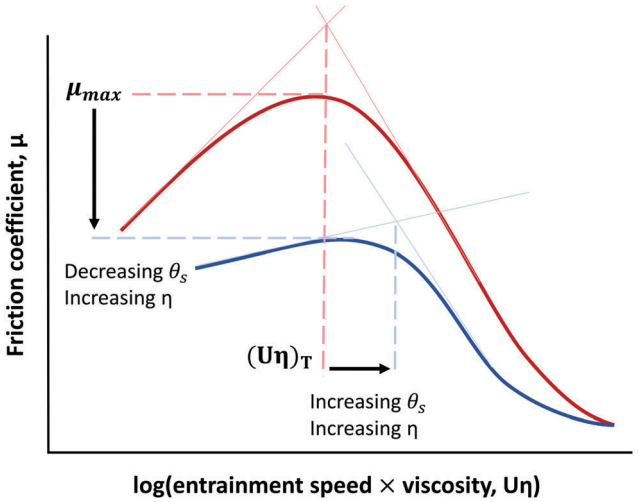

Fig. 9 Schematic showing the generalised trends in tribological behaviour as influenced by lubricant viscosity and static contact angle. High lubricant viscosity and wettability reduce the friction coefficient over a wide range of reduced velocities, and these properties also govern the critical transition reduced velocity, $(U\eta)_T$. These lubricant effects arise from the complex interplay between the four friction mechanisms depicted in Fig. 8.

5. Conclusions

Lubricant viscosity and static wetting are shown to have a considerable effect on the tribological profiles of glycerol–water and glycerol–ethanol–water systems in smooth and rough viscoelastic contacts over a wide range of reduced velocity values. In both cases, the friction coefficient decreases with increasing lubricant viscosity, attributed to fluid–substrate interactions and their impact on viscoelastic energy dissipation at multiple length scales. It is proposed that the influence of fluid viscosity on lubrication within the smooth contact is governed by dewetting and squeeze-out dynamics molecular-scale (interfacial) viscoelastic effects, whereby more viscous fluids reduce friction by inhibiting fluid removal from the contact zone and slowing down the molecular bonding/debonding events responsible for adhesion. Lubricant properties have less effect on interfacial friction in the rough contact due to the rapid removal of fluid *via* percolation channels at low speeds; however, an additional component of friction arises from fluid–asperity interactions within the rough contact during the mixed lubrication transition, which stimulate additional rubber hysteresis at the asperity-scale, altering the general shape of the Stribeck curve. Conventional scaling with lubricant viscosity is shown to be insufficient to achieve a master curve and indirect viscosity effects on lubrication need to be considered when interpreting tribological data. These findings give rise to numerous avenues for future research (experimental, theoretical and numerical) focussed on the influence of fluid–substrate interplay on friction mechanisms within soft contacts, particularly for lubricant systems that exhibit greater rheological complexity (*e.g.* viscoelastic fluids, particle suspensions). The insights generated from such studies have the potential to be applied in the engineering of novel materials, systems and products with targeted functionality, as well as providing an enhanced understanding of natural lubrication processes.

Abbreviations

PDMS	Polydimethylsiloxane
PTFE	Polytetrafluoroethylene
SRR	Slide-to-roll ratio

Acknowledgements

The authors would like to acknowledge funding from The University of Queensland (UQ Advantage Scholarship) and the Australian Postgraduate Award (APA Scholarship), as well as support *via* the Australian Research Council Linkage Grant (ARC LP140100952) and PepsiCo (USA). Gratitude is also extended to colleagues from the Rheology, Tribology and Biointerfaces research group at UQ for insightful discussions, especially Dr Gleb Yakubov and Grace Dolan.

References

1 A. E. Kovalev, M. Varenberg and S. N. Gorb, *Soft Matter*, 2012, **8**, 7560–7566.
2 G. A. Ateshian, *J. Biomech.*, 2009, **42**, 1163–1176.
3 M. Scaraggi and G. Carbone, *Adv. Tribol.*, 2012, **2012**, 12.
4 J. Chen and J. R. Stokes, *Trends Food Sci. Technol.*, 2011, **25**, 4–12.
5 R. A. de Wijk and J. F. Prinz, *Food Quality and Preference*, 2005, **16**, 121–129.
6 M. E. Malone, I. A. M. Appelqvist and I. T. Norton, *Food Hydrocolloids*, 2003, **17**, 763–773.
7 N. Selway and J. R. Stokes, *Annu. Rev. Food Sci. Technol.*, 2014, **5**, 373–393.
8 C. J. Hooke and P. Huang, *Proc. Inst. Mech. Eng., Part J*, 1997, **211**, 185–194.
9 A. A. Elsharkawy, *Wear*, 1996, **199**, 45–53.
10 J. H. H. Bongaerts, K. Fourtouni and J. R. Stokes, *Tribol. Int.*, 2007, **40**, 1531–1542.
11 J. R. Stokes, L. Macakova, A. Chojnicka-Paszun, C. G. De Kruif and H. H. J. De Jongh, *Langmuir*, 2011, **27**, 3474–3484.
12 D. A. Garrec and I. T. Norton, *Food Hydrocolloids*, 2013, **33**, 160–167.
13 J. de Vicente, H. A. Spikes and J. R. Stokes, *J. Tribol.*, 2006, **128**, 795–800.
14 D. M. Dresselhuis, H. Klok, M. A. C. Stuart, R. de Vries, G. A. van Aken and E. H. A. de Hoog, *Food Biophysics*, 2007, **2**, 158–171.
15 G. A. van Aken, M. H. Vingerhoeds and R. A. de Wijk, *Food Hydrocolloids*, 2011, **25**, 789–796.
16 J. de Vicente, J. R. Stokes and H. A. Spikes, *Tribol. Int.*, 2005, **38**, 515–526.
17 M. Scaraggi and B. N. J. Persson, *Tribol. Int.*, 2014, **72**, 118–130.
18 Y. B. Chernyak and A. I. Leonov, *Wear*, 1986, **108**, 105–138.
19 A. Schallamach, *Wear*, 1963, **6**, 375–382.

20 F. P. Bowden and D. Tabor, *The Friction and Lubrication of Solids*, Clarendon Press, Oxford, 1964.
21 A. M. Bueche and D. G. Flom, *Wear*, 1959, **2**, 168–182.
22 K. C. Ludema and D. Tabor, *Wear*, 1966, **9**, 329–348.
23 K. A. Grosch, *Proc. R. Soc. London, Ser. A*, 1963, **274**, 21–39.
24 S. Sills, K. Vorvolakos, M. Chaudhury and R. Overney, in *Fundamentals of Friction and Wear*, ed. E. Gnecco and E. Meyer, Springer Berlin Heidelberg, 2007, ch. 30, pp. 659–676, DOI: 10.1007/978-3-540-36807-6_30.
25 J. A. Greenwood and D. Tabor, *Proc. Phys. Soc.*, 1958, **71**, 989.
26 J. C. Berg, *An introduction to interfaces & colloids: the bridge to nanoscience*, World Scientific, New Jersey, 2010.
27 S. Sills, K. Vorvolakos, M. K. Chaudhury and R. M. Overney, in *Fundamentals of Friction and Wear*, ed. E. Gnecco and E. Meyer, Springer Berlin Heidelberg, Berlin, Heidelberg, 2007, pp. 659–676, DOI: 10.1007/978-3-540-36807-6_30.
28 K. Vorvolakos and M. K. Chaudhury, *Langmuir*, 2003, **19**, 6778–6787.
29 H. Zeng, J. Huang, Y. Tian, L. Li, M. V. Tirrell and J. N. Israelachvili, *Macromolecules*, 2016, **49**, 5223–5231.
30 A. Einstein, *Ann. Phys.*, 1906, **19**, 371–381.
31 P. Debye, *Polar Molecules*, Dover, New York, 1929.
32 B. Lorenz, B. A. Krick, N. Rodriguez, W. G. Sawyer, P. Mangiagalli and B. N. J. Persson, *J. Phys.: Condens. Matter*, 2013, **25**, 445013.
33 J. Drelich, J. L. Wilbur, J. D. Miller and G. M. Whitesides, *Langmuir*, 1996, **12**, 1913–1922.
34 T. D. Blake and Y. D. Shikhmurzaev, *J. Colloid Interface Sci.*, 2002, **253**, 196–202.
35 X.-D. Pan, *Polymer Adhesion, Friction, and Lubrication*, John Wiley & Sons, Inc., 2013, ch. 11, pp. 443–499, DOI: 10.1002/9781118505175.